Stevens, V. L., Sloan, R. A., Chindandali, P., Wedmore, L. N. J., Salomon, G. W., & Muir, R. A. (2021). The Entire Crust can be Seismogenic: Evidence from Southern Malawi. *Tectonics*, *40*(6), [e2020TC006654]. https://doi.org/10.1029/2020TC006654

The Entire Crust can be Seismogenic: Evidence from Southern Malawi

V. L. Stevens[1], R. A. Sloan[1], P. R. Chindandali[2], L. N. J. Wedmore[3], G. W. Salomon[1]and R. A. Muir[1]

[1]Geological Sciences Department, University of Cape Town, Rondebosch, 7700, South Africa
[2]Geological Survey Department, P.O. Box 27, Zomba, Malawi
[3]Department of Earth Sciences, University of Bristol, Bristol, UK

Key Points:

- Microseismicity occurs throughout the entire crust in southern Malawi
- Microseismicity highlights a normal fault plane all the way down to 35 km
- The entire crust is capable of hosting earthquakes (i.e. not the jelly sandwich model)

Corresponding author: Victoria L. Stevens, victoria.stevens@uct.ac.za

Abstract

The Bilila-Mtakataka Fault (BMF), at the southern end of the western branch of the East African Rift System (EARS), has been used in various scaling relation studies and arguments about the strength of the lithosphere. We present evidence for a similar, though more degraded, frontal scarp on the graben-bounding synthetic Chirobwe-Ntcheu Fault (CNF), showing that this fault is active simultaneously with the BMF. We deployed 17 geophones for ∼60 days around the southern end of Lake Malawi, across the footwall and hangingwall of the BMF. Continuous microseismicity can be seen from the surface to ∼35 km depth highlighting a plane dipping ∼42° east. Lower-crustal earthquakes have previously been found in the EARS, and based on location and focal mechanism have been hypothesized to occur on planes that line up with the surface traces of large faults. However, no previous study of the EARS has revealed a fault plane throughout the crust that shows seismicity along its full length from the surface to the base of the crust. Rather, the lack of seismicity seen at mid-lower crustal depths, has led some people to the 'jelly sandwich' hypothesis. Our results show that the entire crust is seismogenic, so support the 'crème brûlée' model. In our two month deployment we recorded 22 aftershocks $M_L \geq 2$ from the 8th March 2018 earthquake 200 km south of our array, seven months after the mainshock, confirming that aftershock sequences in regions of low strain have a long duration, and could be the main component of seismicity in slowly straining regions.

Plain Language Summary

We set out instruments around the southern end of Lake Malawi to detect earthquakes. There is a large fault in the area, the Bilila-Mtakataka Fault, where a large earthquake has occurred previously. Evidence for this comes from a ∼110 km-long cliff, averaging 14 m high, showing movement in a past earthquake, which probably happened thousands of years ago. We found a ∼80 km-long cliff at the base of another large nearby fault, called the Chirobwe-Ntcheu Fault. This means that large earthquakes could also occur on this fault. There was no previous evidence for what these faults looked like beneath the surface, or whether many small earthquakes were happening on it. We discovered that these faults are probably a continuous straight line underground, highlighted by small earthquakes that occur from the surface to almost 35 km depth. This shows that a very large earthquakes could occur, reaching from this large depth all the way to the surface. We recorded, in two months, 40 events from the coal fields at Tete, Mozam-

bique, where previously residents have complained that coal blasting creates shaking and has formed cracks in their homes. The events that we detected are the likely cause of these cracks.

1 Introduction

The largely amagmatic western branch of the East African Rift System (EARS) has been noted for unusually deep earthquakes ($\geq$ 25 km), long normal faults ($\sim$100 km) and wide grabens ($\sim$50 km) (e.g., Ebinger et al., 1993; J. Jackson & Blenkinsop, 1997; Craig et al., 2011). The largest known normal-faulting continental earthquake, 1910 Ruwka M7.4 earthquake, occurred along the 180 km long Kanda Fault (Vittori et al., 1997) in this region. These observations have been used to hypothesize that the lithosphere here is particularly cold and strong, leading to a large elastic thickness, which controls other parameters such as maximum fault length, graben width and seismogenic depth (Buck, 1991; J. Jackson & Blenkinsop, 1993; C. H. Scholz & Contreras, 1998; Ebinger et al., 1999). Unlike the EARS, most other areas of continental extension, for example Greece and western Turkey, have seismicity restricted to the upper crust and a seismogenic depth of 10–15 km (e.g., Chen & Molnar, 1983; J. A. Jackson & White, 1989; Maggi et al., 2000).

The processes by which tectonic strain is accumulated vary with depth in the crust, and this depth variation is controlled by a combination of factors including crustal composition, geothermal gradient and tectonic strain rate (e.g., Burov, 2011; Tamura et al., 2020; Zielke et al., 2020). In some countries, such as the USA, dense networks of broadband seismometers accurately record the location of decades worth of microseismic data which can be used to refine the geometry of models of active faulting, and can help to infer the depth extent of velocity-weakening behavior which can lead to large and damaging earthquakes (e.g., Smith-Konter et al., 2011; Ross et al., 2020). These data are a crucial input to seismic hazard models that can be used to estimate the likely size and frequency of future earthquakes.

In Southern Africa, seismic infrastructure is sparse, and consequently knowledge of the distribution of microseismicity is limited to a small number of case studies led by international research groups (e.g., Lavayssière et al., 2019; Keir et al., 2009; Ebinger et al., 2017, 2019). To make matters worse, there is ample evidence that the processes by which tectonic strain accumulates in this area are significantly different from many more

rapidly deforming and better studied regions. This leads to challenges in making reasonable evidence-based assumptions in seismic hazard models. Moderate-magnitude earthquakes analyzed using teleseismic recordings on the globally distributed stations reveal that such events can occur in the lower crust and uppermost mantle in some areas of the East African Rift. However, the small number of such events that occur in a particular area during our observational period limits our ability to make evidence-based assumptions about individual structures, and has led to heated debates on subjects like the presence or absence of an aseismic layer in the mid-lower crust. Such debates potentially have important implications for hazard modeling.

1.1 The East African Rift System

In the EARS, Yang and Chen (2010); Accardo et al. (2018) and others have observed a bimodal distribution of seismicity, with peaks in the upper crust ($\sim$15$\pm$5 km depth), and around the depth of the Moho (35$\pm$3 km), with few earthquakes in between, leading to the persistence of the 'jelly sandwich' model, which suggests that the lower crust is weak and deforms in a ductile manner. However, others (e.g., Maggi et al., 2000; Emmerson et al., 2006; J. Jackson, 2002; J. Jackson et al., 2008) have used the discovery that the deeper earthquakes principally occur within the lower crust to suggest the 'crème brûlée' rheological model of the lithosphere, with the strength of the lithosphere assumed to lie entirely in the crust. In this model, in most areas earthquakes occur only in the upper crust, though in some areas with stronger lithosphere, such as the EARS and Baikal Rift, earthquakes occur throughout the crust. These two models leads to different explanations for deeper earthquakes - either compositionally strong lower crust, or strong upper mantle, potentially combined with a weakness penetrating to depth, or in certain locations high strain rates associated with magmatism.

The EARS has long been a typical example of an geographic region with either lower crustal earthquakes or unusually deep continental earthquakes, thick lithosphere, and a half-graben style of rifting (e.g., Ebinger et al., 1989, 1993; J. Jackson & Blenkinsop, 1997; Priestley & McKenzie, 2013; Lavier, 2002). Rifting in the western branch of the EARS started $\sim$25 Ma (Roberts et al., 2012). The Malawi Rift is at the southern end of the largely amagmatic western branch of the southern EARS (Ebinger et al., 1993), which extends 900 km from Tanzania in the north to Mozambique in the south. It is characterized by alternating half-grabens with segmented border faults, roughly 120 km long,

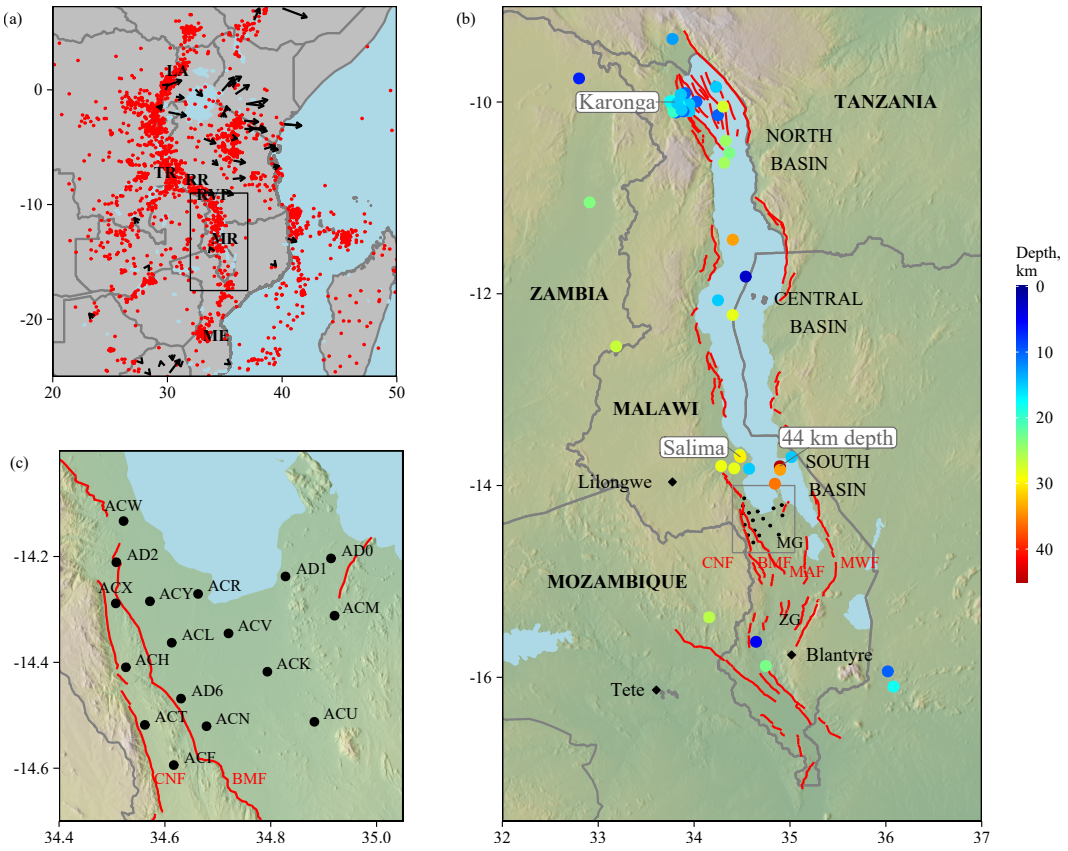

Figure 1. Setting. a) Earthquakes from the IRIS catalog (1966-2020) as red dots, with b) outlined by the black box. Black arrows show GPS velocities in the fixed-Nubian reference frame (Saria et al., 2014). LA = Lake Albert, TR = Tanganyika Rift, RR = Rungwe Rift, RVP = Rukwa Volcanic Province, MR = Malawi Rift, ME = Machaze Earthquake.

b) Malawi Rift, with red lines showing mapped faults, and small black dots showing our station locations. Colored dots show earthquakes from the ISC-EHB catalog (Engdahl et al., 1998, 2020) color-coded by depth. These depths have significant errors; half of the 42 earthquakes plotted have depth errors of $\geq$15 km. Earthquakes mentioned in the text are labeled. Black box marks the location of c). Country borders are shown in gray. Earthquakes mentioned in the text are labeled in pale gray. BMF = Bilila-Mtakataka Fault, CNF = Chirobwe-Ntcheu Fault, MAF = Malombe Fault, MWF = Mwanjage Fault, MG = Mankanjira Graben, ZG = Zomba Graben.

c) Location of our geophones. Red line shows the active faults. Faults from Williams et al. (2019) and references within. Colored background is elevation from SRTM 30 m DEM.

with throws of 7–8 km in the northern section and decreasing towards the south (e.g., Ebinger et al., 1987). Intrarift faulting may take up 10–50% of the deformation along the rift (e.g., Muirhead et al., 2019; Wedmore, Biggs, et al., 2020).

For southern Malawi, the extension rates are about 2 mm/yr, roughly ENE-WSW in orientation (Stamps et al., 2018; Saria et al., 2014). The Malawi Rift propagated southward (C. Scholz et al., 2020), with the start of rifting in the North Basin of Lake Malawi around 9–20 Ma (Ebinger et al., 1993; Mortimer et al., 2016), and the Central Basin roughly 4.6 Ma (McCartney & Scholz, 2016). Earthquake mechanisms from the gCMT catalog (Ekström et al., 2012) are all normal faulting, striking similar to the border faults, NNW-SSE and N-S. Depth estimates of teleseismic earthquakes in this region are up to 44± 4 km in the southern part of the Lake (Yang & Chen, 2010; Craig et al., 2011), though the deep seismicity of the Malawi Rift is similar to elsewhere in the Western Branch of the EARS (Nyblade & Langston, 1995; Yang & Chen, 2010; Craig et al., 2011; Lavayssière et al., 2019). The largest earthquakes in instrumental times in the Malawi rift are the 1989 Salima earthquake of M_{w}6.1, at 35±5 km depth (with a foreshock the day before of M_{w}5.5) (J. Jackson & Blenkinsop, 1993), and the 2009 Karonga earthquake sequence of four M_{w}5.5–6 earthquakes, at 6–10 km depth (Biggs et al., 2010).

1.2 The Bilila-Mtakataka Fault

The Bilila-Mtakataka Fault is one of the world's longest continental normal faults, at 110 km long. It is an east-dipping fault that lies at the Western edge of the Mankanjira Graben, in the hangingwall of a major escarpment, the Chirobe-Ntcheu Fault, at the south end of Lake Malawi (Fig. 1). The largest measured scarp height is 34 m, with an average of 14±8 m (J. Jackson & Blenkinsop, 1997; Hodge et al., 2018). Original studies suggested that, based on the continuous nature and similar offset all the way along the 110 km long scarp, that it was formed in one large, $\sim M_{\mathrm{w}}$8, earthquake (J. Jackson & Blenkinsop, 1997). Recent work suggest it may have been formed in two earthquakes of $\geq$ M_{w}7.5 (Hodge et al., 2020), and morphological variations along scarp define six 10–40 km long segments with surface dips of 30–55° (Hodge et al., 2018). No strike-slip offsets have been found in the field or in the DEM (J. Jackson & Blenkinsop, 1997) so it is assumed to be purely normal. Its trend averages 150°, roughly perpendicular (∼78°) to the local minimum horizontal stress inferred from earthquake focal mechanisms in the

Malawi rift (Williams et al., 2019). Hodge et al. (2020) used diffusion modeling of the scarp to estimate an age of roughly 6.4 ± 4 ka.

J. Jackson and Blenkinsop (1993) connected the unusual (for continental normal faults) characteristics of the BMF rupture with the presence of a seismogenic fault extending through the entire crust. However, before this study there was no evidence of earthquakes in the lower crust south of Lake Malawi, and even to the north, evidence for lower crustal seismicity was limited to six events which occurred at 25–40 km and were interpreted as potentially upper mantle events which may not indicate a seismogenic lower crust.

The major rift-bounding escarpment, the Chirobe-Ntcheu Fault, has been less studied. It has been suggested that it consists of three segments, and has a total height of 300-1000 m (J. Jackson & Blenkinsop, 1997), however since no frontal scarp has previously been noted, it was not known if this fault was still active.

2 Methods

We deployed 17 geophones to southern Malawi from October to December 2018 (see Fig. 1c). These were 3-component PE-6/B 4.5 Hz geophones made by SENSOR Nederland, chosen for their low-cost and high robustness, to demonstrate that low-cost methods suitable for developing countries can give valuable results. Site conditions varied from very dry hard-packed soil on the valley floor, to looser soil above the footwall of the BMF. Most stations recorded for ∼60 days apart from stations ACR and ACV which suffered damage within the first five days (see Fig. S1a for number of picks recorded per station). We used the coincidence trigger algorithm from ObsPy (Beyreuther et al., 2010) to automatically detect possible event. P and S arrivals were picked manually using SEISAN (Havskov & Ottemöller, 1999). The earthquakes were located using HYPOCENTER (Lienert & Havskov, 1995). Local magnitudes, ML, were found by estimating maximum displacement amplitudes on the seismograms, after having used our geophone responses to simulate an original Wood-Anderson seismometer (Anderson & Wood, 1925). We use the distance correction term of (Hutton & Boore, 1987), with the amplitude attenuation parameters found for Northern Malawi (Ebinger et al., 2019).

VELEST (Kissling, 1995) was used for the 69 earthquakes within our focus area (an area surrounding our geophone network, box (i) in Fig. 2) to solve simultaneously

for the earthquake locations and velocity structure. This program calculates a best-fitting crustal velocity structure by minimizing the residuals between the predicted and observed arrival times. To account for lateral heterogeneities in the crustal structure, VELEST calculates corrections for each station (see Fig. S1b). For each of the 69 earthquakes used, they had a minimum of seven arrivals, of which at least two P and three S.

There are fewer earthquakes at depths which have ray paths that sample the Moho, and teleseismic events are not picked up by the geophones, so we cannot constrain the depth of the Moho or velocity of the upper mantle well. If we vary the Moho depths, and corresponding higher velocities, from 35 to 50 km, we find no change in the location or depths of our final earthquakes. If we test a Moho depth of 30 km, meaning some earthquakes are now in the mantle, the locations found for 10 earthquakes change slightly, with a small increase in depth on average of 1.4 km, but no change to the overall picture. We chose a final model with a Moho depth of 35 km based on the location of the deepest earthquakes found, and comment on this further in the discussion. We use a sub-Moho P wave velocity of 8 km/s, based on previously found velocities from travel-time analysis of regional earthquakes (Lavayssière et al., 2019) and regional tomography models (O'Donnell et al., 2013).

We test the stability of our velocity model by changing the input velocities of the layers by ± 1 km, and seeing how well VELEST finds a solution that converges back to the final velocity model chosen (Fig. S2). The model converges back to within 0.3 km/s for most layers apart from those deeper than 30 km, where there are only 10 earthquakes, and the difference in velocities between models is 0.5 km/s. If these higher and lower velocity models are used to find earthquake locations, their depths change by 0.7 km on average, and no more than $\sim$3 km (see Figures S3b,c). We also test the stability of the earthquake depths by varying the depths randomly by 0–10 km from their current position, and seeing if VELEST locates the earthquakes back to the same position. We find that it does (see Fig. S3a), and most variation occurs for the shallower earthquakes.

An average Vp/Vs ratio of 1.72 was found over our study area from constructing a Wadati diagram (see Fig. S4). This is slightly lower than the value of 1.74 found from a similar study in Tanzania (Lavayssière et al., 2019), and lower than the values of 1.75–1.81 found by receiver function analysis in our region, with 1.75 the value found closest to our network (Sun et al., 2021) (see Fig. S5a). The upper crust is preferentially sam-

pled by the local earthquakes of our study, whereas receiver function studies sample the entire crust. This may explain the discrepancy in values found, since significant variation in Vp/Vs ratios can occur within the crust, especially in highly fractured areas (e.g., Gentile et al., 2000; Zhao & Xu, 2013). We show how the depths found would change based on Vp/Vs ratio of 1.75 and 1.81 in Fig. S6. For the extreme Vp/Vs ratio of 1.81 more than 85% of earthquakes would change depth by less than 5 km, and for a Vp/Vs ratio of 1.75 roughly 95% of earthquakes would change depth by less than 2 km.

For our final velocity model, the average residual for these 69 earthquakes in our focus areas was 0.08 s. We use the same velocity model outside our focus area, where we find 129 earthquakes, with average residuals of 0.4 s. For two areas of interest (boxes 1 and 2 on Fig. 2a), both further than 200 km from our network, we set the depths to zero as they are too far away to be located reliably, and we can only constrain the rough geographical locations of these earthquakes.

3 Results and Discussion

We located a total of 198 earthquakes (for table of locations, see Supplementary Information ds01). Increased anthropogenic noise during the day led to twice as many earthquakes being found between 5pm and 5am than during the daylight hours. We found that the geophone stations nearest the center of the rift were in general the least noisy, even at night time. The average horizontal uncertainty for those in our focus area is 1.8 km, and the depth uncertainty is 2.1 km. Outside our focus area, horizontal uncertainties increase to ∼20 km, and depth uncertainties, excluding those that were fixed to zero depth, to ∼5 km. Even though these earthquakes are less well located, before concentrating on our focus area, we discuss two interesting clusters of seismicity that do not depend on precise locations - those in boxes 1 and 2 in Fig. 2a.

3.1 Earthquakes Outside Focus Area

3.1.1 Mining Related Events

We find a cluster of 40 events, with M_L2.4–3.1, near to the coal mines of Tete, Mozambique, about 220 km away from our geophone network (see Fig. 2a Box 1 and Fig. S7). Their locations are not that well clustered, but spread out forming an arc equidistant to the network, as their distance away from the network is better constrained that the

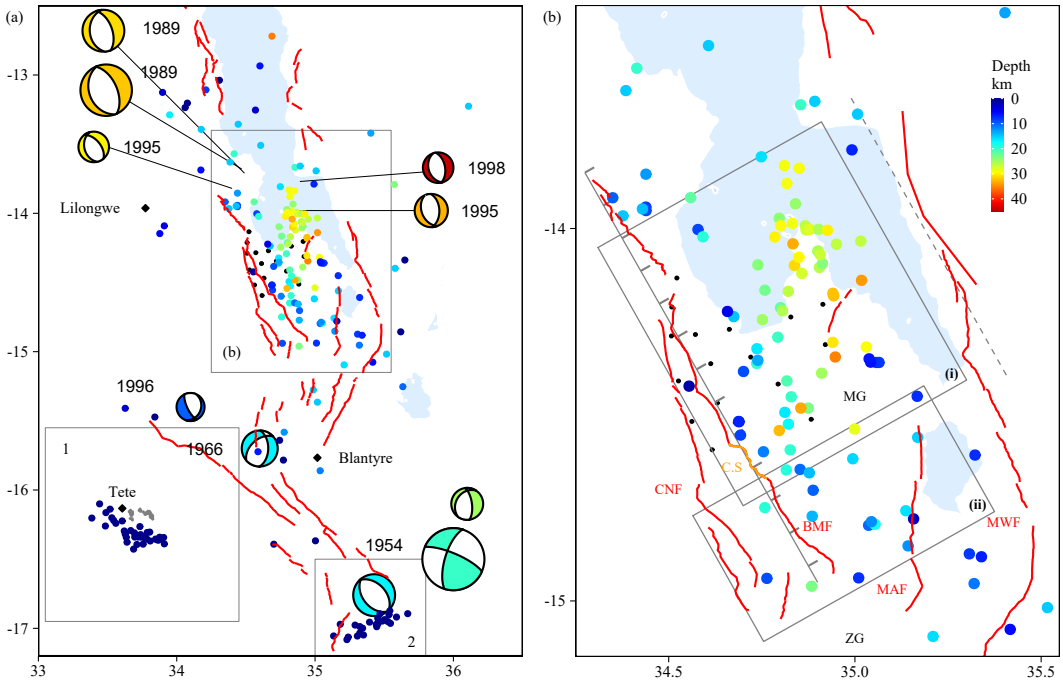

Figure 2. Locations of earthquakes found from this study. Red lines are faults from Williams et al. (2021) and Laõ-Dávila et al. (2015). a) Larger scale. Box (b) shows the area of (b). Box 1 shows the coal-mining related events, and the extent of Fig. S7a, with the gray areas showing the area of open-cast coal mining near Tete. Box 2 shows the aftershocks of the 2018 earthquake, and the extent of Fig. S8a. Earthquakes in both these areas have had their depths set to 0 km due to their location far outside our network. Previous earthquake focal mechanisms from Craig et al. (2011) are shown with dates, apart from the 2018 mechanism which is from the gCMT catalog (Ekström et al., 2012). b) Box (i) shows earthquakes in what we call our focus area, which are plotted in Fig. 3d. Box (ii) shows earthquakes further from our array, plotted in the cross-section of Fig. S10. Straight line with spikes shows our simplified surface trace of the BMF, from which perpendicular distances are measured in Fig. 3d. Dashed gray line shows the simplified surface trace of a western-dipping border fault on the eastern side of the rift, also shown in Fig. 3d as a dashed line. Small black dots are our station locations. BMF = Bilila-Mtakataka Fault. CNF = Chirobwe-Ntcheu Fault. MAF = Malombe Fault. MWF = Mwanjage Fault MG = Makanjira Graben, ZG = Zomba Graben. C.S = Chitsulo Segment of the BMF, highlighted in orange.

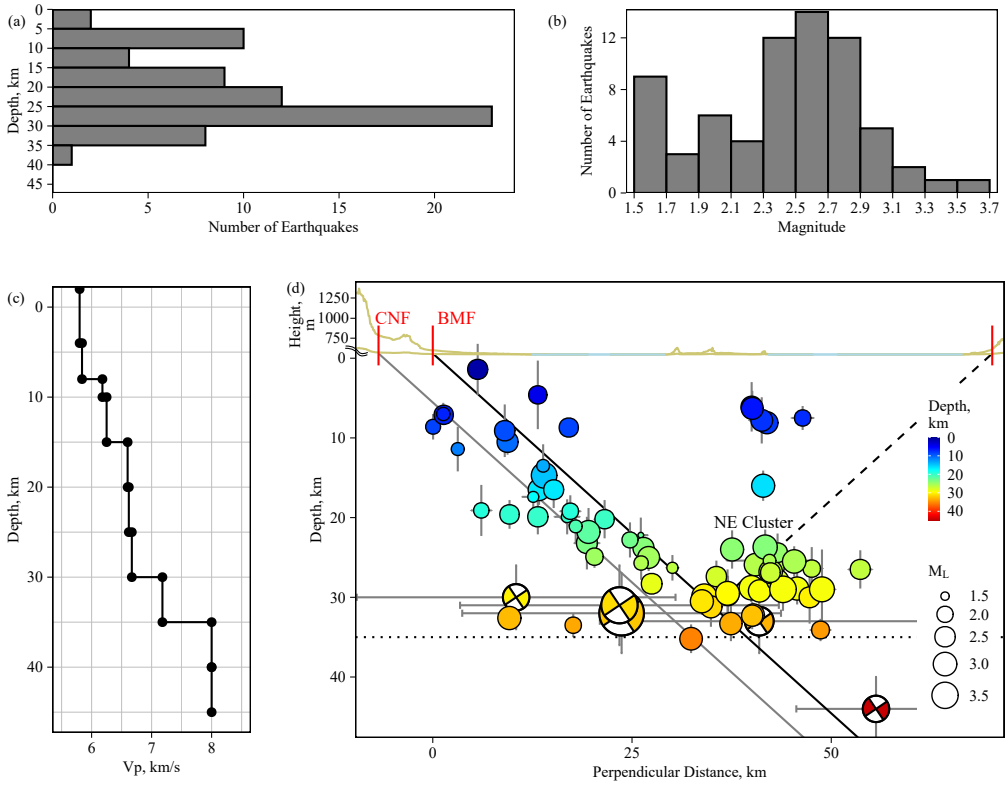

Figure 3. Earthquakes from the box (i) in Fig. 2b). a) Depths, b) Magnitudes, c) The final velocity structure chosen, d) Cross-section with perpendicular distance from the surface trace of the simplified BMF (Bilila-Mtakataka Fault), shown as the gray line with spikes in Fig. 2b). Solid colored dots show the earthquakes found in this study. Earthquakes with focal mechanisms are from Craig et al. (2011), who used an average Vp of 6.5 km/s, similar to our average Vp to 35 km of 6.4 km/s. Grey horizontal and vertical lines show the standard error in horizontal location and depth respectively. Solid black dipping line shows the best fitting straight-line to the earthquakes within 40 km perpendicular distance, fixed at the surface trace, and dips at 42°. Dashed black dipping line shows a hypothetical fault plane dipping from the surface trace of a fault on the eastern side of the lake to intersect with the cluster of earthquakes around 25–30 km depth, and dips at 48°. Black horizontal dotted line at 35 km shows the maximum depth of earthquakes found in our study, and a possible location of the Moho. Short vertical red lines show the positions of the surface traces of the BMF, CNF (Chirobwe-Ntcheu Fault) and the border fault on the eastern edge of the rift. Brown and blue line above 0 km shows the topography, with brown showing solid ground, and blue showing the lake surface, with a vertical exaggeration of both ×1 and ×10. We show similar cross-sections that result from using different Vp/Vs ratios in Fig. S9. A cross-section for box (ii) is shown in Fig. S10.

precise direction. These coal mines are open cast, where blasting is used to remove rock, and local residents have blamed the blasting for causing ground shaking and cracks in their houses (Temper et al., 2015). Based on the timing of these events, we think they are directly related to blasting: The events occur only between 10am and 16pm (Fig. S7d), almost 50% occur within a few minutes of the hour (Fig. S7e), and none occur on Sundays (Fig. S7c). Due to their low magnitude and low density of permanent seismometers in the region, this cluster of events has not been picked up by global networks.

3.1.2 Southern Aftershocks

Another cluster of 22 earthquakes with M_{L} 1.8–4 can be seen in Fig. 2a, Box 2, and Fig. S8. These are near to the M_{w}5.5 earthquake of March 8th 2018, which occurred roughly seven months before our deployment started. Based on its location and normal focal mechanism, this earthquake probably occurred at the SE end of the 85 km long Thyolo Fault (Wedmore, Williams, et al., 2020), a NE-striking border fault in the Lower Shire Graben. In the two years since, global catalogs have detected six earthquakes in the area with magnitudes M_{b}4.4–4.7, and in the two month period starting seven months after the mainshock, we detected 22 earthquakes with magnitudes 2–4. This is far more aftershocks than typically occur after an event of this magnitude in more rapidly deforming regions. For example, after three similar magnitude earthquakes in California on strands of the San Andreas Fault, only 0–4 aftershocks of magnitude > 2 are found in any two month period more than six months after the earthquake (see Fig. S11). Long-duration aftershock sequences have been seen elsewhere in the region, e.g. in Mozambique, at the southern end of the EARS, the 2006 M_{w}7.0 Machaze earthquake is still producing aftershocks, which include the 2016 M_{w}5.6 Zinave earthquake (Lloyd et al., 2019) ten years after the mainshock. In many slower deforming regions, the density of seismometers is lower, so the long duration of aftershocks is more difficult to see, though it may be a common feature (e.g., Stein & Liu, 2009). This may be expected since the stress change caused by a large event in a slowly deforming region takes a longer time to be overwhelmed by the stress change due to tectonic loading of the fault, and so the number of earthquakes takes a longer time to decay down the background rate.

3.2 Earthquakes In Focus Area

The earthquakes in our focus area are fairly evenly distributed throughout the network, though there is a cluster towards the north-east (Fig. 2b). Earthquakes increase in depth towards the center of the lake and in cross-section delineate a planar structure dipping at ∼42° which has not been imaged before (Fig. 3). Earthquakes highlight this plane along its entire length, with no gap in seismicity between the surface and the deepest earthquakes at 35 km depth. This contrasts with the aftershocks of the intra-rift Karonga 2009 earthquake, which were all ≤ 15 km depth (Gaherty et al., 2019), highlighting the possibility that intra-rift faults may have substantially smaller down-dip rupture widths than rift-bounding structures. However, it is similar to other local studies, where most earthquakes at the northern end of Lake Malawi are found up to depths of ∼34 km (Albaric et al., 2009; Ebinger et al., 2019), and beneath the Tanganyika rift, where earthquakes are found at all depths continuously down to ∼42 km, the local depth of the Moho (Lavayssière et al., 2019). Even though these studies find earthquakes at continuous depths until the Moho, they are not all on the same fault plane. On the border faults, Lavayssière et al. (2019) see earthquakes from 0–20 km, a gap, and then clusters at lower crustal depths. Assuming dips of 50–60°, they then line the patches up to surface traces of the faults (e.g., Lavayssière et al., 2019). A possible reason why these studies see no continuous plane, but we do, might be due to station geometry. The Lavayssière et al. (2019) study had a station spacing of 50–100 km, rather than our more focused study over a small area, with a station spacing of ∼10 km. Their study was also constrained to have all their stations on the footwall due to the position of Lake Taganyika above the hangingwall, whereas most of ours were on the hangingwall, so directly above the fault plane, and many of the earthquakes at mid-crustal depths were smaller than those at 30–35 km. It could also be that the recent larger earthquakes e.g. 1989 M_w6.1 Salima earthquake and the three more recent ≥ M_w4.7 events have transferred stress to the BMF and/or CNF, causing current microseismicity.

3.2.1 The Bilila-Mtakataka (BMF) and Chirobwe-Ntcheu Faults (CNF)

The BMF and CNF are synthetic east-dipping normal faults, both roughly 100 km long. The BMF frontal scarp has been known for some time (J. Jackson & Blenkinsop, 1997), however nothing similar has previously been noted for the CNF. Using a 12.5 m resolution TanDEM-X DEM we find a semi-continuous steep frontal scarp at the base

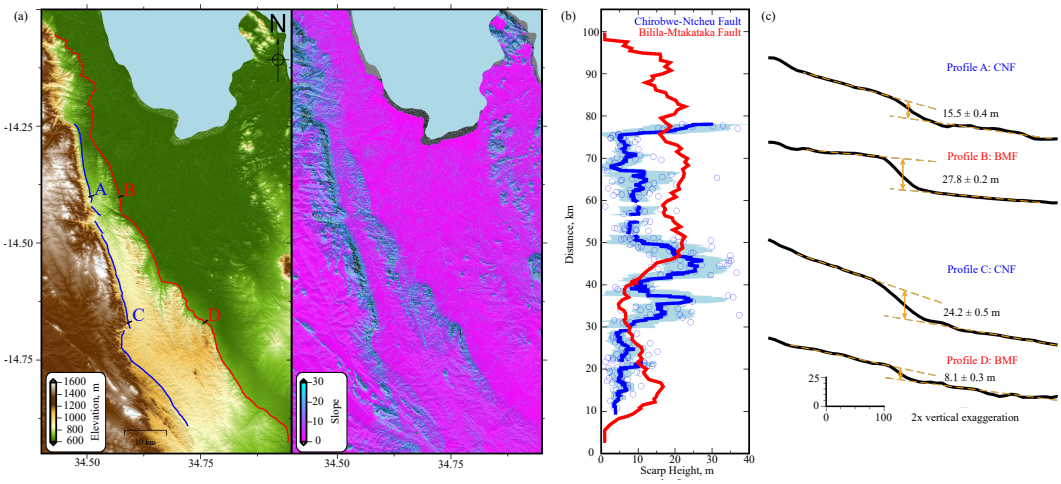

Figure 4. The Chirobwe-Ntcheu Fault. a) Elevation and Slope. Chirobwe-Ntcheu Fault is shown in blue, Bilila-Mtakataka Fault is shown in red. b) Scarp height along the frontal scarp of the CNF using the method of Wedmore, Biggs, et al. (2020). Hollow circles show individual measurements across the scarp using TanDEM-X DEM. This DEM has a horizontal resolution of 12.5 m, and a vertical mean error of ±0.2 m (RMS error <1.4 m (Wessel et al., 2018)). The solid line shows the 3 km wide moving medians, and the paler shading represents the 1σ error. Scarp height along the BMF from Hodge et al. (2018). c) Elevation profiles across the CNF and BMF scarps, with locations shown in a).

of the CNF escarpment with a mean height of ∼12 m and a maximum height of ∼30 m (Fig. 4). In places, the scarp offsets recently deposited alluvial fan material, suggesting that the fault has been active in the late-Quaternary. This shows that the CNF is the border fault in the region, in contrast to previous interpretations (e.g., Hodge et al., 2018). The CNF scarp itself is more degraded and less steep than the BMF (see Fig.4c), suggesting an older age for the most recent event. Additionally, the straighter fault segments and larger topographic step across the CNF compared to the BMF (Figs. 4a and 3d) suggest that the CNF is more mature.

In our focus area, the surface expression of the CNF and BMF are just a few km apart, and our dipping plane of seismicity cannot distinguish between either of these faults (see Fig. 3d). Further south, the BMF moves towards the center of the rift, and ends up ∼20 km further east than the CNF. Here we see a hint that two separate planes of seismicity corresponding to the CNF and BMF can be distinguished (see Fig. S10). It is possible that the BMF merges into the CNF below the surface. This interpretation is likely in the north due to the closeness of their surface expression in that area and the relatively low dip of ∼42° observed. It may be that the slip on the basin bounding structure (CNF) exploits different structural weaknesses in the upper crust during different events, forming the two distinct surface traces. For simplicity of language, in the subsequent discussion we assume that the seismicity occurs on the BMF: The two structures are likely either similar in geometry, or the BMF is a splay-fault branching off from the CNF. Indeed, the scarp height measurements may suggest that these two faults are working together; when the scarp is high on the BMF, it is lower on the CNF, and vice versa (see Fig. 4b). Therefore, which fault the seismicity is on does not influence the arguments that follow.

The dip of the plane of seismicity, ∼42°, is within the observed range for large normal faults of 30–65° (Collettini & Sibson, 2001). Slightly steeper dips of ∼60° have been measured from surface scarps of other border faults in the region (Wheeler & Rosendahl, 1994; Ebinger et al., 1989; Williams et al., 2019), and seismic reflection profiling in the North Basin of Lake Malawi shows faults of dip ∼50–60° (Accardo et al., 2018). The dips of focal mechanisms range from 30–60°, showing that the dips are never shallow. It can be difficult to determine which nodal plane is the fault plane due to lack of surface rupture and sparse regional instrumentation not allowing the detection of smaller aftershocks

which might delineate a fault plane. However, if we look only at east-dipping planes within our study area, they are all in the range 50–56°.

The 1989 M_w6.1 Salima earthquake is one such ambiguous earthquake. The focal mechanism suggests the fault plane dips either $34 \pm 5°$ west or $56 \pm 5°$ east. J. Jackson and Blenkinsop (1993) located this earthquake teleseismically, finding an epicenter almost 40 km north of the surface expression of the BMF, with a horizontal uncertainty of ∼20 km (J. Jackson & Blenkinsop, 1993). Its strike of $156 \pm 25°$ matches very well with the BMF. Partly based on the macroseismic epicenter, J. Jackson and Blenkinsop (1993) hypothesized that this earthquake was on the more gently dipping, west-dipping border fault with a surface trace on the east-side of the rift. We hypothesize that the actual epicenter was ∼10 km east of where it was located teleseismically, and that it lies at the northern end of the BMF. At this location the BMF has no surface expression, but its strike and dip agree well with the Salima earthquake focal mechanism. Additionally, we favor the steeper, east-dipping nodal plane since we do not see such a low dip of 34±5° for other border faults in the EARS. J. Jackson and Blenkinsop (1993) found a centroid depth of 32 km. They could not determine whether this earthquake occurred in the crust or mantle, or whether the fault it occurred on was a shear zone located only in the lower crust, or a seismogenic plane throughout the entire crust. We suggest that it occurred in the crust on a seismogenic plane similar to that which we find, extending from ≥30 km to the surface, which was their preferred hypothesis.

In the previous absence of other information, Hodge et al. (2018) modeled the subsurface geometry of the BMF by finding the geometry that best fit the variation in surface offsets along the scarp. They found that if the fault was assumed to be continuous at depth, the best fitting plane would have a very low dip of 22°. They also modeled the fault as two sub-faults at depth, with a gap at the Chitsulo segment (shown in orange on Fig. 2b) where the scarp height is almost zero. In this case, a dip of 46° for the northern segment and 38° for the southern segment was found to fit best. The dip of ∼42° that we find agrees with this second model. We also notice a change in the seismicity pattern across the Chitsulo segment, where to the south there are no earthquakes deeper than 20 km. In this location, the Malombe Fault overlaps with the BMF (see Fig. S10), perhaps influencing the characteristics of the BMF seismicity. Another possible reason for the changing characteristics could be related to the increased distance from the CNF and a corresponding change from being a 'boundary', to intrarift fault.

Previously, morphological variations in the surface trace of the BMF have been used to define six segments each 10–40 km long along this scarp (Hodge et al., 2020). We do not have enough earthquakes to be able to comment on how these might be represented, if at all, at depth. However, we see in general that the BMF seems to be fairly continuous at depth, in a similar manner to other faults around the world which are segmented at the surface, but continuous at depth (e.g., Nicol et al., 2005; Worthington & Walsh, 2017).

The average strike of the BMF is about 150°, which is mis-oriented by 26±5° with respect to the direction of minimum strain of $86 \pm 5°$ (Saria et al., 2014). The EARS is influenced by pre-existing structure and geology (e.g., Morley, 2010). Unlike the Eastern Branch of the EARS where magmatic weakening is important for strain localization, for the Western Branch pre-existing structures are more important. (e.g. Muirhead et al., 2019). The mis-orientation of the BMF with regard to strain is probably a case of exploiting a previous deep-seated crustal weakness (Williams et al., 2019). This weakness may then rotate the local strain field, as has been proposed previously for this fault (Williams et al., 2019; Hodge et al., 2018) and others in the EARS (Corti et al., 2013; Morley, 2010). Pre-existing structures and foliations which influence the direction of maximum principal stress may also cause the initiation of faults at angles less than 60° (Morley, 2010).

3.2.2 The NE Cluster

The deep cluster in the north east (labeled on Fig. 3d) has three potential explanations. The first is that these earthquakes occur preferentially near an intersection between the BMF and a west-dipping border fault on the other side of the rift, and this tectonic complexity increases stress nearby. Some of the earthquakes here may be occurring on this oppositely dipping border fault. Clustering around the intersection of conjugate faults has also been seen in other areas of thick crust such as Scandinavia (Lindblom et al., 2015), and for other normal faults, such as those in Italy (Walters et al., 2018). Clustering around fault intersections has also been seen more locally, as in aftershocks of the Karonga earthquake sequence, though the intersection here included intrabasinal faults, and was at ∼10 km depth (Biggs et al., 2010; Gaherty et al., 2019). Deeper clustering of earthquakes, at 25–35 km depth, near suspected fault intersections, has also been

hypothesized for the North and Central Basin of Lake Malawi (Ebinger et al., 2019) and for the Tanganyika Rift (Lavayssière et al., 2019).

A second explanation is that these are aftershocks of previous larger earthquakes. The 1989 M_w6.1 Salima earthquake, located 40 km north of the northern end of the BMF (J. Jackson & Blenkinsop, 1993) has a ∼20 km horizontal uncertainty in location, and could in fact lie near the location of the current cluster, at about 30–35 km depth. The 1995 and 1998 earthquakes of M_w4.9 and M_w4.7 respectively, also at depths of 30–35 km, which may themselves be aftershocks of the Salima earthquakes, could also cause aftershocks in this region. As mentioned previously, in slowly deforming regions, aftershock sequences can last a long time (Stein & Liu, 2009). In our study area, the location of all the larger earthquakes may have been influenced by the intersection of the eastern-dipping border fault from the opposite side, or may just have preferentially nucleated at the base of the crust. The fact that there are more deeper earthquakes in the north may be because this is the area nearest the larger previous earthquakes.

A third explanation is that the fault is listric and becomes flat at this location. However, there are multiple lines of evidence that the faults in the EARS are planar; the steep-dipping focal mechanisms of deep earthquakes, depth to detachment calculations, and tilt of blocks at least 50 km wide, which suggests that border faults are planar to great depths (Muirhead et al., 2019; Biggs et al., 2010). Restored balanced cross-sections across Lake Tanganyika fit best planar, not listric faults (Muirhead et al., 2019), and clusters of seismicity at depth tend to line up with straight line projections from the surface traces of known faults (e.g., Lavayssière et al., 2019; Ebinger et al., 2019). Additionally, normal faults with such a low angle may not be seismically active (e.g., Collettini & Sibson, 2001), and a half-graben style of faulting, rather than listric faulting tends to be typical for cold, strong areas (Lavier, 2002; Olive et al., 2014). We therefore do not favor this explanation.

A final related explanation is that the planar high-angle normal fault roots into a microseismically active detachment at the brittle-plastic transition (e.g., Rigo et al., 1996), and it is the microseismicity on this structure that we are seeing. However, the focal mechanisms of larger earthquakes do not fit well with this explanation.

3.2.3 Low Intrabasinal Deformation

In the EARS large border faults, with surface offsets of up to a few kilometers, define the edge of the rift basins. Within the basin itself, intrabasinal faults and folds occur. One surprising feature that our seismicity shows is the lack of intrabasinal deformation away from the main fault. There is also only one area which has plausible topographic expression of intra-basin faulting (see Fig. 3d topographic profile). We see some shallow seismicity outside our focus area to the SE on the Malombe Fault, a 55 km long east-dipping normal fault with a scarp with average offsets of ∼7 m (Hodge et al., 2019), supporting its current activity. We see a small cluster of three earthquakes at < 10 km depth at 35.1°E, 14.35°S, which may be related to a northern extension of the Malombe Fault, or some other smaller intrabasinal fault. We see no seismicity on the Mwanjage Fault, to the SE on the eastern edge of the rift, although it is further away so small earthquakes would not be detected by our deployment.

Apart from the cluster of three shallow earthquakes, we see no other internal deformation in our focus area. This is in contrast to the North and Central Basins of Lake Malawi, where reflection profiling shows many intrabasinal faults 15–44 km long, spaced ∼10 km apart (e.g., Mortimer et al., 2007), and they are thought to accommodate ∼20–25% of the extension (Shillington et al., 2020). The four $M_w > 5.5$ earthquakes of the Karonga sequence also occurred on intrabasinal faults (Biggs et al., 2010), showing that the hanging wall further north is actively breaking up. In the Central Basin, at least for the past 1.3 Ma, border faults and intrabasinal faults have been moving synchronously (McCartney & Scholz, 2016). In our study area there is less throw on the boundary faults (∼1 versus ∼6–7 km, Laõ-Dávila et al. (2015)), so lower intrabasinal stresses, and the rift may also be younger, so strain has not migrated from the border faults to the basin yet (e.g., Muirhead et al., 2019).

However, also further south, in the Zomba Graben, intrabasinal faults of similar length and spacing to those in the North Basin, are thought to take up 55±24% of extensional strain (Wedmore, Biggs, et al., 2020). Further north than Lake Malawi in the Tanganyika Rift, only 10% of extensional strain is seen on intrabasinal faults as compared to border faults (Muirhead et al., 2019), which is similar to the low intrabasin seismicity we find here. Since the rift is thought to be propagating southward (e.g., Ebinger et al., 1993; C. Scholz et al., 2020), but there seem to be alternating areas of low and high

intrabasinal deformation, the age of the rift cannot be the sole component controlling the migration of faulting from the borders to within the basin (e.g., Muirhead et al., 2019). One previous suggestion is that the angle of the border faults and rifts compared to the direction of extension may also be important, and that more deformation would be concentrated on the border faults when the rift is perpendicular to the direction of regional extension (Shillington et al., 2020). In our study area, the strike of the BMF is almost perpendicular to the extension direction, meaning we would expect a lower amount of intrabasinal extension here compared to e.g. the Northern Malawi Rift.

3.2.4 Moho depth

All of the earthquakes that we find are at depths of ≤ 35 km, however one M_w4.7 earthquake found by Yang and Chen (2010) was located at 44±4 km depth, with a horizontal uncertainty of ∼10 km (see Fig. 1b) for location of this earthquake). Yang and Chen (2010) used a simple velocity model of Vp = 6.2 km/s in a 30 km thick crust, below which Vp = 7.8 km/s. This gives an average Vp to 45 km of 6.7 km/s, compared to our average value of 6.8 km/s. The location and dip of 53° for this earthquake could fit on the straight subsurface extension of the BMF fault (see Fig, 3), however it is ∼10 km deeper than any earthquake we find. We examine the implications for this earthquake either being in the crust or the mantle.

If this earthquake is in the crust, the Moho would have to be at a similar depth, ∼44 km. This is deeper than other regional studies that have found the Moho depth in the EARS and the surrounding cratons, which would be expected to have a deeper Moho: using receiver function analysis Sun et al. (2021) found a Moho depth of 39.4±2.7 km below the Malawi rift, and using ambient noise tomography Wang et al. (2019) estimated a Moho depth of 36–40 km for southern Malawi. From seismic reflection surveys a Moho depth of 37.5 km for the Rukwa Rift in Tanzania was found (Kim et al., 2009), crust in the nearby Tanzania craton has also been found to have a similar depth, of only 36 ± 4 km (Last et al., 1997; Julià et al., 2005), and the depth of the Moho beneath the northern Malawi rift ranges from 38–42 km, similar to that of the surrounding Proterozoic terranes (Borrego et al., 2018). The global crustal model CRUST1.0 (Laske et al., 2012) suggests that Moho depths along the EARS axis are 5 km less than intact Tanzanian craton, which was 36 km. However the gravity based study of Njinju et al. (2019) suggests that the crust within the rift is at least thick as the surrounding areas. At our array, the

CRUST1.0 model suggests Moho depths are roughly 33–37 km, and the Njinju et al. (2019) model suggests depths of ∼40 km (see Fig. S12a).

Yang and Chen (2010) suggest this earthquake is in the mantle, due to its large depth and because they see underside reflections off the Moho in the coda that suggest it is 12± 2 km below the Moho. That would fit with our microseismicity being continuous to the Moho, at ∼35 km. The upper mantle could be particularly cold and strong here, as the rift goes through Archean craton, with the thick lithosphere shielding it from the hotter mantle below (e.g., Craig et al., 2011). Based on its location and focal mechanism, it could be on a continuation of the BMF into the mantle, perhaps as a predominantly ductile aseismic shear zone that nevertheless sometimes concentrates enough strain to produce medium-sized earthquakes, similar to what has been seen elsewhere in the geological record (Campbell et al., 2020). Deep seismicity, of up to 60 km, has been seen elsewhere in the EARS, though these are all smaller, and potentially related to magmatism (e.g., Lindenfeld et al., 2012; Ebinger et al., 2019; Lavayssière et al., 2019).

3.3 Strength of the Crust and Lower-Crustal Earthquakes

Unlike other studies of the Western Branch of the EARS, which find peaks in seismicity at shallower depths, with a second smaller peak near the Moho (e.g., Albaric et al., 2009; Yang & Chen, 2010) and argue for a 'jelly sandwich' rheology, we find seismicity continuously along a border fault at all depths, with an abrupt stop at the probable depth of the Moho, around ∼35 km. We suggest that the potential lower crustal peak seen previously is from the clusters at depth being caused by fault intersections, which if the border faults were 60 km apart and dipped at 45°, would intersect at 30 km depth.

Another explanation is a low-angle microseismically active detachment at the brittle-ductile transition. Or, there could be a higher probability of larger earthquakes nucleating at the base of the crust either due to the higher stresses found here (e.g., Shi et al., 2020), or the presence of mafic material (Julià et al., 2005), and the earthquakes we see now are aftershocks of these. In the mid-crust we see mainly smaller earthquakes, suggesting that it may more difficult for larger earthquakes to nucleate here. However, the presence of small earthquakes shows that there are at least velocity weakening asperities within the mid-crust capable of generating microseismicity. It is impossible to state conclusively that the presence of microseismicty indicates that the entire crust will

rupture in larger earthquakes, as they may represent small velocity weakening asperities set within a velocity-strengthening shear zone, or alternatively be the result of elevated strain rates associated with previous events. Nevertheless, the distribution of these earthquakes does support the interpretation that the northern segment of the rift-bounding fault is seismogenic throughout the entire crust. In other parts of the EARS, magmatism-related seismicity in the lower crust may cause earthquakes at these larger depths.

Various hypothesis have been used to explain lower crustal seismicity in the EARS: high-viscosity mafic material (Nyblade & Langston, 1995; Albaric et al., 2009; Hellebrekers et al., 2019); old, strong, anhydrous, low-temperature crust (thermally shielded by the thick lithosphere, see Fig. S12c) (J. A. Jackson et al., 2004; Craig et al., 2011); localized zones of weak rheology i.e. a fault, leading to a high strain rate, within a strong elastic lower crust (Fagereng, 2013; Hodge et al., 2018). While all these possibilities may occur simultaneously, we see that border faults do represent zones of weakness extending to the base of the crust (or possibly further), which is the hypothesis of Fagereng (2013). One condition for this hypothesis was that the surrounding crust must be strong, which is evidenced from the large effective elastic thickness of 20–30 km seen in this region (Ebinger et al., 1991; Pérez-Gussinyé et al., 2009).

3.4 Seismic Hazard

Our results confirm that the BMF is seismogenic from the surface to the lower crust, $\sim$ 35 km. We hypothesized that the 1989 M_{w}6.1 Salima earthquake occurred on this fault, nucleating at the deeper end. This earthquake did not rupture the surface (J. Jackson & Blenkinsop, 1993), though the high 14±8 m scarp at the surface trace of the BMF, and the abundant active scarps observed in the Zomba and Lower Shire Grabens (Wedmore, Biggs, et al., 2020; Wedmore, Williams, et al., 2020), shows that some earthquakes do, with probable magnitudes of M_{w}7–8 (J. Jackson & Blenkinsop, 1997; Hodge et al., 2020). Our results are compatible with an earthquake nucleating at the base of the crust, near where we see the cluster of microseismicity, and propagating all the way to the surface, with no barrier to rupture in the form of a ductile mid-lower crust. The seismic hazard study of Poggi et al. (2017) assumed a maximum magnitude earthquake of 7.9 and a maximum source depth of 40 km for the Malawi Rift zone, roughly consistent with our findings. No M_{w}8 continental normal faulting earthquake has even been observed (see Fig. S13 for global distribution of normal-faulting earthquakes $\geq$ M_{w}6.5); the fact that it

may be possible here is a result of the large seismogenic thickness and associated fault length and widths. Our study shows the strongest evidence yet for the large seismogenic thickness for one of these major East African faults, and the BMF can be seen as the type locality for this behavior.

Fault scaling relations suggest that earthquakes $\geq M_{\mathrm{w}}7$ are also possible elsewhere in Malawi (Williams et al., 2021; Wedmore, Biggs, et al., 2020), and further north along Tanganyika border faults (Lavayssière et al., 2019). Similarly long border faults and deep seismicity are seen all the way to Lake Albert (Rosendahl et al., 1992), towards the northern end of the western branch of the EARS. The large seismogenic depth may only start to decrease far to the south. The 2006 $M_{\mathrm{w}}7.0$ Machaze earthquake, at the very southern end of the EARS, almost 800 km further south than our deployment, had deep aftershocks suggesting the seismogenic thickness here is more than 20 km (Lloyd et al., 2019), though perhaps less than the $\sim$35 km found here in southern Malawi. From scaling relations (e.g., Leonard, 2010), the larger the width of an earthquake, the longer in length its rupture may be, and for a fault dipping 42°, increasing the seismogenic depth from 25 to 35 km leads to roughly double the moment release if the entire fault plane slipped.

We cannot directly comment on age of the most recent rupture on either the BMF or CNF. Hodge et al. (2020) proposed an age of 6.4 ± 4 ka for the scarp based on diffusion modeling, though assumed a dip of 60° for the initial scarp angle. We see that the fault dip is lower, at 42°, though we cannot exclude shallow steepening, and if the initial scarp angle was initially lower, diffusion modeling could give a younger age. The CNF scarp appears to be older than the BMF, which suggests an age of more than 6.4 ± 4 ka. Based on extension rates and potential strain distribution patterns, Hodge et al. (2015) calculate a recurrence time of $\geq$ 3.4 ka for the BMF, however they assumed that the CNF was not active and therefore not accumulating strain. If the faults accumulate strain at the same rate, the recurrence time for the individual faults would then be ≥ 6.8 ka. Given that the CNF has not ruptured so recently as the BMF, we might expect the next large earthquake to occur on the CNF.

We think that many of the earthquakes observed may be aftershocks. The previously recorded moderate magnitude earthquakes ($\sim M_{\mathrm{w}}4.7$) in our area occurred in 1995 and 1998, six and nine years after the $M_{\mathrm{w}}6.1$ Salima earthquake respectively. Based on

the relatively short time interval after the Salima earthquake and their proximity (20–40 km from Salima centroid), they could be aftershocks. These may then go on to produce further aftershocks, potentially influencing the NE cluster of microseismicity we see. The Ufipa M_w6.8 and Rungwe M_w6.2 earthquakes in 1919, and the Rukwa M_w6.2 in 1922 are probably aftershocks of the 1910 Ruwka M_w7.4 event (Ambraseys & Adams, 1992). There have also been nine earthquakes with $M_w > 5.2$ in the area since 1975, recorded in the instrumental record. If most instrumental seismicity in slowly deforming regions is aftershocks (e.g., Stein & Liu, 2009), then it is not a good indicator of future hazard, and it becomes even more important to study the geomorphology and geodetic data (e.g., Hodge et al., 2015).

4 Conclusions

We found microseismicity highlighting a plane dipping $\sim 42°$ extending from the surface to almost 35 km depth. This shows that the entire crust is seismogenic, and a large earthquake could initiate at depth and then propagate to the surface. Instead of a ductile, weak lower crust (e.g., Chen & Molnar, 1983; Yang & Chen, 2010), the surrounding crust must be strong for weaknesses such as faults to host earthquakes (Fagereng, 2013). We suggest that some of the deeper seismicity clusters in the amagmatic EARS are caused by intersection of planar border faults on either side of the rift at overlaps, which if the rift is 70–80 km wide, and the faults dip 42°, the intersection would occur at 35–40 km depth, near the base of the crust. It could also be that many larger earthquakes are deep and maybe start at this intersection, and the continuing aftershocks are also deep. The lower crust is not fully ductile or aseismic here, but deep earthquakes occur because of localization of strain on a weakness that penetrates the strong surrounding crust (Fagereng, 2013).

We find little evidence for intrabasin seismicity, though significant intrabasin deformation is seen in the northern basin of Lake Malawi (Mortimer et al., 2007) and the Zomba graben to the south (Wedmore, Biggs, et al., 2020), both of which strike differently to most of the Malawi Rift. Aftershocks are continuing at a fairly high rate after the 8th March 2018 M_w5.5 event, in line with areas of low strain having long duration aftershocks, which potentially make up most of the earthquakes recorded in the EARS, and may be a significant source of future hazard. Although the global catalogs found no

earthquakes in the study area during our deployment, we detected 198 earthquakes with magnitudes 0.2–4.0.

We tested to see whether a focused short-term (two-month) deployment of (relatively) low-cost geophones could provide useful information on the geometry and seismic potential of a particular structure in a relatively low-strain-rate environment. The study, run by researchers based in South Africa and Malawi, used relatively simple analysis techniques available in the open source SEISAN package which has been widely adopted by regional researchers. We have demonstrated that this approach has considerable utility, successfully defining the geometry of a major structure and helping to support assumptions which have been made in seismic hazard analyses. We suggest that similar deployments, run by local researchers and migrating along the rift, may be one of the most realistic mechanisms for mapping out variations in the subsurface geometry and potentially rheological behavior with the current levels of research investment.

Acknowledgments

This work is supported by the EPSRC-Global Challenges Research Fund PREPARE project 1045 (EP/P028233/1). VLS and RAM were additionally supported by the Claude Leon Postdoctoral Fellowship. RAS acknowledges financial support from the NRF (118831, 110780). We thank the Geological Survey Department, Zomba, Malawi and Patricia Kapolo for her help in the field. We thank Juliet Biggs, Åke Fagereng and Jack Williams for useful suggestions. We also thank Raymond Durrheim and an anonymous reviewer whose comments and suggestions helped improve this manuscript. Earthquake location data are available in the supplementary material and have also been archived with the ZivaHub repository at: `http://doi.org/10.25375/uct.13405460` with the CC BY 4.0 license.

References

Accardo, N. J., Shillington, D. J., Gaherty, J. B., Scholz, C. A., Nyblade, A. A., Chindandali, P. R., ... Wambura Ferdinand, R. (2018). Constraints on Rift Basin Structure and Border Fault Growth in the Northern Malawi Rift From 3-D Seismic Refraction Imaging. *J. Geophys. Res. Solid Earth*, *123*(11), 10,003–10,025. doi: 10.1029/2018JB016504

Albaric, J., Déverchère, J., Petit, C., Perrot, J., & Le Gall, B. (2009). Crustal rheology and depth distribution of earthquakes: Insights from the central and

southern East African Rift System. *Tectonophysics*, *468*(1-4), 28–41. doi: 10.1016/j.tecto.2008.05.021

Ambraseys, N. N., & Adams, R. D. (1992). Reappraisal of major African earthquakes, south of 20N, 1900-1930. *Tectonophysics*, *209*(1-4), 293–296. doi: 10.1016/0040-1951(92)90036-6

Anderson, J. A., & Wood, H. O. (1925). Description and theory of the torsion seismometer. *Bull. Seismol. Soc. Am.*, *15*(1), 1–72.

Beyreuther, M., Barsch, R., Krischer, L., Megies, T., Behr, Y., & Wassermann, J. (2010, may). ObsPy: A python toolbox for seismology. *Seismol. Res. Lett.*, *81*(3), 530–533. doi: 10.1785/gssrl.81.3.530

Biggs, J., Nissen, E., Craig, T., Jackson, J., & Robinson, D. P. (2010). Breaking up the hanging wall of a rift-border fault: The 2009 Karonga earthquakes, Malawi. *Geophys. Res. Lett.*, *37*(11). doi: 10.1029/2010GL043179

Borrego, D., Nyblade, A. A., Accardo, N. J., Gaherty, J. B., Ebinger, C. J., Shillington, D. J., ... Tepp, G. (2018). Crustal structure surrounding the northern Malawi rift and beneath the Rungwe Volcanic Province, East Africa. *Geophys. J. Int.*, *215*(2), 1410–1426. doi: 10.1093/gji/ggy331

Buck, W. R. (1991). Modes of continental lithospheric extension. *J. Geophys. Res.*, *96*(B12), 20161–20178. doi: 10.1029/91jb01485

Burov, E. B. (2011, aug). *Rheology and strength of the lithosphere* (Vol. 28) (No. 8). Elsevier. doi: 10.1016/j.marpetgeo.2011.05.008

Campbell, L. R., Menegon, L., Fagereng, & Pennacchioni, G. (2020). Earthquake nucleation in the lower crust by local stress amplification. *Nat. Commun.*, *11*(1), 1–9. doi: 10.1038/s41467-020-15150-x

Chen, W.-P., & Molnar, P. (1983). Focal depths of intracontinental and intraplate earthquakes and their implications for the thermal and mechanical properties of the lithosphere. *J. Geophys. Res.*, *88*(B5), 4183–4214. doi: 10.1029/jb088ib05p04183

Collettini, C., & Sibson, R. H. (2001, oct). Normal faults, normal friction? *Geology*, *29*(10), 927–930. doi: 10.1130/0091-7613(2001)029⟨0927:NFNF⟩2.0.CO;2

Corti, G., Philippon, M., Sani, F., Keir, D., & Kidane, T. (2013, oct). Re-orientation of the extension direction and pure extensional faulting at oblique rift margins: Comparison between the Main Ethiopian Rift and

laboratory experiments. *Terra Nov.*, *25*(5), 396–404. Retrieved from http://doi.wiley.com/10.1111/ter.12049 doi: 10.1111/ter.12049

Craig, T. J., Jackson, J. A., Priestley, K., & Mckenzie, D. (2011, apr). Earthquake distribution patterns in Africa: Their relationship to variations in lithospheric and geological structure, and their rheological implications. *Geophys. J. Int.*, *185*(1), 403–434. doi: 10.1111/j.1365-246X.2011.04950.x

Ebinger, C. J., Deino, A. L., Drake, R. E., & Tesha, A. L. (1989, nov). Chronology of volcanism and rift basin propagation: Rungwe volcanic province, East Africa. *J. Geophys. Res.*, *94*(B11), 15785–15803. doi: 10.1029/jb094ib11p15785

Ebinger, C. J., Deino, A. L., Tesha, A. L., Becker, T., & Ring, U. (1993, oct). Tectonic controls on rift basin morphology: evolution of the northern Malawi (Nyasa) Rift. *J. Geophys. Res.*, *98*(B10), 17821–17836. doi: 10.1029/93jb01392

Ebinger, C. J., Jackson, J. A., Foster, A. N., & Hayward, N. J. (1999, apr). Extensional basin geometry and the elastic lithosphere. *Philos. Trans. R. Soc. A Math. Phys. Eng. Sci.*, *357*(1753), 741–765. doi: 10.1098/rsta.1999.0351

Ebinger, C. J., Karner, G. D., & Weissel, J. K. (1991, dec). Mechanical strength of extended continental lithosphere: Constraints from the Western Rift System, East Africa. *Tectonics*, *10*(6), 1239–1256. doi: 10.1029/91TC00579

Ebinger, C. J., Keir, D., Bastow, I. D., Whaler, K., Hammond, J. O., Ayele, A., ... Hautot, S. (2017, dec). *Crustal Structure of Active Deformation Zones in Africa: Implications for Global Crustal Processes* (Vol. 36) (No. 12). Blackwell Publishing Ltd. doi: 10.1002/2017TC004526

Ebinger, C. J., Oliva, S. J., Pham, T. Q., Peterson, K., Chindandali, P., Illsley-Kemp, F., ... Mulibo, G. (2019, aug). Kinematics of Active Deformation in the Malawi Rift and Rungwe Volcanic Province, Africa. *Geochemistry, Geophys. Geosystems*, *20*(8), 3928–3951. doi: 10.1029/2019GC008354

Ebinger, C. J., Rosendahl, B. R., & Reynolds, D. J. (1987, sep). Tectonic model of the Malaŵi rift, Africa. *Tectonophysics*, *141*(1-3), 215–235. doi: 10.1016/0040-1951(87)90187-9

Ekström, G., Nettles, M., Dziewoński, A. M., & Dziewoński, A. M. (2012, jun). The global CMT project 2004-2010: Centroid-moment tensors for 13,017 earth-

quakes. *Phys. Earth Planet. Inter.*, *200-201*, 1–9. doi: http://dx.doi.org/10.1016/j.pepi.2012.04.002

Emmerson, B., Jackson, J., McKenzie, D., & Priestley, K. (2006, dec). Seismicity, structure and rheology of the lithosphere in the Lake Baikal region. *Geophys. J. Int.*, *167*(3), 1233–1272. doi: 10.1111/j.1365-246X.2006.03075.x

Engdahl, E. R., Di Giacomo, D., Sakarya, B., Gkarlaouni, C. G., Harris, J., & Storchak, D. A. (2020, jan). ISC-EHB 1964–2016, an Improved Data Set for Studies of Earth Structure and Global Seismicity. *Earth Sp. Sci.*, *7*(1). doi: 10.1029/2019EA000897

Engdahl, E. R., van der Hilst, R., & Buland, R. (1998, jun). Global teleseismic earthquake relocation with improved travel times and procedures for depth determination. *Bull. Seismol. Soc. Am.*, *88*(3), 722–743.

Fagereng, Å. (2013, aug). Fault segmentation, deep rift earthquakes and crustal rheology: Insights from the 2009 Karonga sequence and seismicity in the Rukwa-Malawi rift zone. *Tectonophysics*, *601*, 216–225. doi: 10.1016/j.tecto.2013.05.012

Gaherty, J. B., Zheng, W., Shillington, D. J., Pritchard, M. E., Henderson, S. T., Chindandali, P. R. N., ... Nettles, M. (2019, mar). Faulting processes during early-stage rifting: seismic and geodetic analysis of the 2009–2010 Northern Malawi earthquake sequence. *Geophys. J. Int.*, *217*(3), 1767–1782. doi: 10.1093/gji/ggz119

Gentile, G. F., Bressan, G., Burlini, L., & De Franco, R. (2000, may). Three-dimensional V(P) and V(P)/V(S) models of the upper crust in the Friuli area (northeastern Italy). *Geophys. J. Int.*, *141*(2), 457–478. Retrieved from `https://academic.oup.com/gji/article/141/2/457/648278` doi: 10.1046/j.1365-246X.2000.00095.x

Havskov, J., & Ottemöller, L. (1999, sep). SeisAn earthquake analysis software. *Seismol. Res. Lett.*, *70*(5), 532–534. doi: 10.1785/gssrl.70.5.532

Hellebrekers, N., Niemeijer, A. R., Fagereng, Å., Manda, B., & Mvula, R. L. (2019, sep). Lower crustal earthquakes in the East African Rift System: Insights from frictional properties of rock samples from the Malawi rift. *Tectonophysics*, *767*, 228167. doi: 10.1016/j.tecto.2019.228167

Hodge, M., Biggs, J., Fagereng, Mdala, H., Wedmore, L. N., & Williams, J. N.

(2020, feb). Evidence From High-Resolution Topography for Multiple Earthquakes on High Slip-to-Length Fault Scarps: The Bilila-Mtakataka Fault, Malawi. *Tectonics*, *39*(2). doi: 10.1029/2019TC005933

Hodge, M., Biggs, J., Fagereng, Å., Elliott, A., Mdala, H., & Mphepo, F. (2019, jan). A semi-automated algorithm to quantify scarp morphology (SPARTA): Application to normal faults in southern Malawi. *Solid Earth*, *10*(1), 27–57. doi: 10.5194/se-10-27-2019

Hodge, M., Biggs, J., Goda, K., & Aspinall, W. (2015, jan). Assessing infrequent large earthquakes using geomorphology and geodesy: the Malawi Rift. *Nat. Hazards*, *76*(3), 1781–1806. doi: 10.1007/s11069-014-1572-y

Hodge, M., Fagereng, Biggs, J., & Mdala, H. (2018, may). Controls on Early-Rift Geometry: New Perspectives From the Bilila-Mtakataka Fault, Malawi. *Geophys. Res. Lett.*, *45*(9), 3896–3905. doi: 10.1029/2018GL077343

Hutton, L. K., & Boore, D. M. (1987). The Ml Scale in Southern California. *Bull. Seismol. Soc. Am.*, *77*(6), 2074–2094.

Jackson, J. (2002). Strength of the continental lithosphere: Time to abandon the jelly sandwich? *GSA Today*, *12*(9), 4–10. doi: 10.1130/1052-5173(2002)012⟨0004:SOTCLT⟩2.0.CO;2

Jackson, J., & Blenkinsop, T. (1993, oct). THE Malaŵi Earthquake of March 10, 1989: DEep faulting within the East African Rift System. *Tectonics*, *12*(5), 1131–1139. doi: 10.1029/93TC01064

Jackson, J., & Blenkinsop, T. (1997, feb). The Bilila-Mtakataka fault in Malaŵi: An active, 100-km long, normal fault segment in thick seismogenic crust. *Tectonics*, *16*(1), 137–150. doi: 10.1029/96TC02494

Jackson, J., McKenzie, D., Priestley, K., & Emmerson, B. (2008, mar). New views on the structure and rheology of the lithosphere. *J. Geol. Soc. London.*, *165*(2), 453–465. doi: 10.1144/0016-76492007-109

Jackson, J. A., Austrheim, H., McKenzie, D., & Priestley, K. (2004, jul). Metastability, mechanical strength, and the support of mountain belts. *Geology*, *32*(7), 625–628. doi: 10.1130/G20397.1

Jackson, J. A., & White, N. J. (1989, jan). Normal faulting in the upper continental crust: observations from regions of active extension. *J. Struct. Geol.*, *11*(1-2), 15–36. doi: 10.1016/0191-8141(89)90033-3

Julià, J., Ammon, C. J., & Nyblade, A. A. (2005, aug). *Evidence for mafic lower crust in Tanzania, East Africa, from joint inversion of receiver functions and Rayleigh wave dispersion velocities* (Vol. 162) (No. 2). Oxford Academic. doi: 10.1111/j.1365-246X.2005.02685.x

Keir, D., Bastow, I. D., Whaler, K. A., Daly, E., Cornwell, D. G., & Hautot, S. (2009, jun). Lower crustal earthquakes near the Ethiopian rift induced by magmatic processes. *Geochemistry, Geophys. Geosystems*, *10*(6), n/a–n/a. doi: 10.1029/2009GC002382

Kim, S., Nyblade, A. A., & Baag, C. E. (2009). Crustal velocity structure of the Rukwa Rift in the western branch of the east african Rift system. *South African J. Geol.*, *112*(3-4), 251–260. doi: 10.2113/gssajg.112.3-4.251

Kissling, E. (1995). *Velest User's Guide* (Tech. Rep.). Zurich: Institute of Geophysics, ETH.

Laõ-Dávila, D. A., Al-Salmi, H. S., Abdelsalam, M. G., & Atekwana, E. A. (2015, dec). Hierarchical segmentation of the Malawi Rift: The influence of inherited lithospheric heterogeneity and kinematics in the evolution of continental rifts. *Tectonics*, *34*(12), 2399–2417. doi: 10.1002/2015TC003953

Laske, G., Masters, G., Ma, Z., & Pasyanos, M. (2012). CRUST1. 0: An updated global model of Earth's crust. In *Geophys res abs* (p. 3743).

Last, R. J., Nyblade, A. A., Langston, C. A., & Owens, T. J. (1997, nov). Crustal structure of the East African Plateau from receiver functions and Rayleigh wave phase velocities. *J. Geophys. Res. Solid Earth*, *102*(B11), 24469–24483. doi: 10.1029/97jb02156

Lavayssière, A., Drooff, C., Ebinger, C., Gallacher, R., Illsley-Kemp, F., Oliva, S. J., & Keir, D. (2019, mar). Depth Extent and Kinematics of Faulting in the Southern Tanganyika Rift, Africa. *Tectonics*, *38*(3), 842–862. Retrieved from `https://onlinelibrary.wiley.com/doi/abs/10.1029/2018TC005379` doi: 10.1029/2018TC005379

Lavier, L. L. (2002, jun). Half graben versus large-offset low-angle normal fault: Importance of keeping cool during normal faulting. *J. Geophys. Res.*, *107*(B6), ETG 8–1. doi: 10.1029/2001jb000513

Leonard, M. (2010). Earthquake fault scaling: Self-consistent relating of rupture length, width, average displacement, and moment release. *Bull. Seismol. Soc.*

Am., *100*(5A), 1971–1988.

Lienert, B. R., & Havskov, J. (1995, sep). A computer program for locating earthquakes both locally and globally. *Seismol. Res. Lett.*, *66*(5), 26–36. doi: 10.1785/gssrl.66.5.26

Lindblom, E., Lund, B., Tryggvason, A., Uski, M., Bödvarsson, R., Juhlin, C., & Roberts, R. (2015, jun). Microearthquakes illuminate the deep structure of the endglacial Pärvie fault, northern Sweden. *Geophys. J. Int.*, *201*(3), 1704–1716. doi: 10.1093/gji/ggv112

Lindenfeld, M., Rümpker, G., Link, K., Koehn, D., & Batte, A. (2012, sep). Fluid-triggered earthquake swarms in the Rwenzori region, East African Rift-Evidence for rift initiation. *Tectonophysics*, *566-567*, 95–104. doi: 10.1016/j.tecto.2012.07.010

Lloyd, R., Biggs, J., & Copley, A. (2019, jan). The decade-long Machaze–Zinave aftershock sequence in the slowly straining Mozambique Rift. *Geophys. J. Int.*, *217*(1), 504–531. doi: 10.1093/gji/ggz033

Maggi, A., Jackson, J. A., McKenzie, D., & Priestley, K. (2000, jun). Earthquake focal depths, effective elastic thickness, and the strength of the continental lithosphere. *Geology*, *28*(6), 495–498. doi: 10.1130/0091-7613(2000)28⟨495:efdeet⟩2.0.co;2

McCartney, T., & Scholz, C. A. (2016, oct). A 1.3 million year record of synchronous faulting in the hangingwall and border fault of a half-graben in the Malawi (Nyasa) Rift. *J. Struct. Geol.*, *91*, 114–129. doi: 10.1016/j.jsg.2016.08.012

Morley, C. K. (2010, sep). Stress re-orientation along zones of weak fabrics in rifts: An explanation for pure extension in 'oblique' rift segments? *Earth Planet. Sci. Lett.*, *297*(3-4), 667–673. doi: 10.1016/j.epsl.2010.07.022

Mortimer, E., Kirstein, L. A., Stuart, F. M., & Strecker, M. R. (2016, dec). Spatiotemporal trends in normal-fault segmentation recorded by low-temperature thermochronology: Livingstone fault scarp, Malawi Rift, East African Rift System. *Earth Planet. Sci. Lett.*, *455*, 62–72. doi: 10.1016/j.epsl.2016.08.040

Mortimer, E., Paton, D. A., Scholz, C. A., Strecker, M. R., & Blisniuk, P. (2007, sep). Orthogonal to oblique rifting: Effect of rift basin orientation in the evolution of the North basin, Malawi Rift, East Africa. *Basin Res.*, *19*(3), 393–407.

doi: 10.1111/j.1365-2117.2007.00332.x

Muirhead, J. D., Wright, L. J., & Scholz, C. A. (2019, jan). Rift evolution in regions of low magma input in East Africa. *Earth Planet. Sci. Lett.*, *506*, 332–346. doi: 10.1016/j.epsl.2018.11.004

Nicol, A., Walsh, J., Berryman, K., & Nodder, S. (2005, feb). Growth of a normal fault by the accumulation of slip over millions of years. *J. Struct. Geol.*, *27*(2), 327–342. doi: 10.1016/j.jsg.2004.09.002

Njinju, E. A., Atekwana, E. A., Stamps, D. S., Abdelsalam, M. G., Atekwana, E. A., Mickus, K. L., ... Nyalugwe, V. N. (2019). Lithospheric Structure of the Malawi Rift: Implications for Magma-Poor Rifting Processes. *Tectonics*, *38*(11), 3835–3853. doi: 10.1029/2019TC005549

Nyblade, A. A., & Langston, C. A. (1995, apr). East African earthquakes below 20 km depth and their implications for crustal structure. *Geophys. J. Int.*, *121*(1), 49–62. doi: 10.1111/j.1365-246X.1995.tb03510.x

O'Donnell, J. P., Adams, A., Nyblade, A. A., Mulibo, G. D., & Tugume, F. (2013, may). The uppermost mantle shear wave velocity structure of eastern Africa from Rayleigh wave tomography: constraints on rift evolution. *Geophys. J. Int.*, *194*(2), 961–978. doi: 10.1093/gji/ggt135

Olive, J. A., Behn, M. D., & Malatesta, L. C. (2014, oct). Modes of extensional faulting controlled by surface processes. *Geophys. Res. Lett.*, *41*(19), 6725–6733. doi: 10.1002/2014GL061507

Pérez-Gussinyé, M., Metois, M., Fernández, M., Vergés, J., Fullea, J., & Lowry, A. R. (2009, sep). Effective elastic thickness of Africa and its relationship to other proxies for lithospheric structure and surface tectonics. *Earth Planet. Sci. Lett.*, *287*(1-2), 152–167. doi: 10.1016/j.epsl.2009.08.004

Poggi, V., Durrheim, R., Tuluka, G. M., Weatherill, G., Gee, R., Pagani, M., ... Delvaux, D. (2017, nov). Assessing seismic hazard of the East African Rift: a pilot study from GEM and AfricaArray. *Bull. Earthq. Eng.*, *15*(11), 4499–4529. doi: 10.1007/s10518-017-0152-4

Priestley, K., & McKenzie, D. (2013, nov). The relationship between shear wave velocity, temperature, attenuation and viscosity in the shallow part of the mantle. *Earth Planet. Sci. Lett.*, *381*, 78–91. doi: 10.1016/j.epsl.2013.08.022

Rigo, A., Lyon-Caen, H., Armijo, R., Deschamps, A., Hatzfeld, D., Makropou-

los, K., ... Kassaras, I. (1996, sep). A microseismic study in the western part of the Gulf of Corinth (Greece): Implications for large-scale normal faulting mechanisms. *Geophys. J. Int.*, *126*(3), 663–688. doi: 10.1111/j.1365-246X.1996.tb04697.x

Roberts, E. M., Stevens, N. J., O'Connor, P. M., Dirks, P. H., Gottfried, M. D., Clyde, W. C., ... Hemming, S. (2012, apr). Initiation of the western branch of the East African Rift coeval with the eastern branch. *Nat. Geosci.*, *5*(4), 289–294. doi: 10.1038/ngeo1432

Rosendahl, B. R., Kilembe, E., & Kaczmarick, K. (1992, oct). Comparison of the Tanganyika, Malawi, Rukwa and Turkana Rift zones from analyses of seismic reflection data. *Tectonophysics*, *213*(1-2), 235–256. doi: 10.1016/0040-1951(92)90261-4

Ross, Z. E., Cochran, E. S., Trugman, D. T., & Smith, J. D. (2020, jun). 3D fault architecture controls the dynamism of earthquake swarms. *Science (80-.).*, *368*(6497), 1357–1361. Retrieved from `https://science.sciencemag.org/content/368/6497/1357https://science.sciencemag.org/content/368/6497/1357.abstract` doi: 10.1126/science.abb0779

Saria, E., Calais, E., Stamps, D. S., Delvaux, D., & Hartnady, C. J. H. (2014, apr). Present-day kinematics of the East African Rift. *J. Geophys. Res. Solid Earth*, *119*(4), 3584–3600. doi: 10.1002/2013JB010901

Scholz, C., Shillington, D., Wright, L., Accardo, N., Gaherty, J., & Chindandali, P. (2020). Intrarift fault fabric, segmentation, and basin evolution of the Lake Malawi (Nyasa) Rift, East Africa. *Geosphere*, *16*. doi: 10.1130/GES02228.1

Scholz, C. H., & Contreras, J. C. (1998, nov). Mechanics of continental rift architecture. *Geology*, *26*(11), 967–970. doi: 10.1130/0091-7613(1998)026⟨0967:MOCRA⟩2.3.CO;2

Shi, Q., Barbot, S., Wei, S., Tapponnier, P., Matsuzawa, T., & Shibazaki, B. (2020, dec). Structural control and system-level behavior of the seismic cycle at the Nankai Trough. *Earth, Planets Sp.*, *72*(1), 343–353. doi: 10.1186/s40623-020-1145-0

Shillington, D. J., Scholz, C. A., Chindandali, P. R., Gaherty, J. B., Accardo, N. J., Onyango, E., ... Nyblade, A. A. (2020, mar). Controls on Rift Faulting in the North Basin of the Malawi (Nyasa) Rift, East Africa. *Tectonics*, *39*(3). doi:

10.1029/2019TC005633

Smith-Konter, B. R., Sandwell, D. T., & Shearer, P. (2011, jun). Locking depths estimated from geodesy and seismology along the San Andreas Fault System: Implications for seismic moment release. *J. Geophys. Res. Solid Earth*, *116*(6), 6401. Retrieved from `https://agupubs.onlinelibrary.wiley.com/doi/full/10.1029/2010JB008117https://agupubs.onlinelibrary.wiley.com/doi/abs/10.1029/2010JB008117https://agupubs.onlinelibrary.wiley.com/doi/10.1029/2010JB008117` doi: 10.1029/2010JB008117

Stamps, D. S., Saria, E., & Kreemer, C. (2018, dec). A Geodetic Strain Rate Model for the East African Rift System. *Sci. Rep.*, *8*(1), 1–9. doi: 10.1038/s41598-017-19097-w

Stein, S., & Liu, M. (2009, nov). Long aftershock sequences within continents and implications for earthquake hazard assessment. *Nature*, *462*(7269), 87–89. doi: 10.1038/nature08502

Sun, M., Gao, S. S., Liu, K. H., Mickus, K., Fu, X., & Yu, Y. (2021). Receiver function investigation of crustal structure in the Malawi and Luangwa rift zones and adjacent areas. *Gondwana Res.*, *89*, 168–176. doi: 10.1016/j.gr.2020.08.015

Tamura, T., Oohashi, K., Otsubo, M., Miyakawa, A., & Niwa, M. (2020, dec). Contribution to crustal strain accumulation of minor faults: a case study across the Niigata–Kobe Tectonic Zone, Japan. *Earth, Planets Sp.*, *72*(1), 7. Retrieved from `https://doi.org/10.1186/s40623-020-1132-5` doi: 10.1186/s40623-020-1132-5

Temper, L., del Bene, D., & Martinez-Alier, J. (2015). Mapping the frontiers and front lines of global environmental justice: the EJAtlas. *J. Polit. Ecol.*, *22*(1), 255–278.

Vittori, E., Delvaux, D., & Kervyn, F. (1997, sep). Kanda fault: A major seismogenic element west of the Rukwa Rift (Tanzania, East Africa). *J. Geodyn.*, *24*(1-4), 139–153. doi: 10.1016/s0264-3707(96)00038-5

Walters, R. J., Gregory, L. C., Wedmore, L. N., Craig, T. J., McCaffrey, K., Wilkinson, M., ... Vittori, E. (2018, oct). Dual control of fault intersections on stop-start rupture in the 2016 Central Italy seismic sequence. *Earth Planet. Sci. Lett.*, *500*, 1–14. doi: 10.1016/j.epsl.2018.07.043

Wang, T., Feng, J., Liu, K. H., & Gao, S. S. (2019, mar). Crustal structure beneath the Malawi and Luangwa Rift Zones and adjacent areas from ambient noise tomography. *Gondwana Res.*, *67*, 187–198. doi: 10.1016/j.gr.2018.10.018

Wedmore, L. N. J., Biggs, J., Williams, J. N., Fagereng, Å., Dulanya, Z., Mphepo, F., ... Mdala, H. (2020). *Active Fault Scarps in Southern Malawi and Their Implications for the Distribution of Strain in Incipient Continental Rifts* (Vol. 39) (No. 3). Blackwell Publishing Ltd. doi: 10.1029/2019TC005834

Wedmore, L. N. J., Williams, J. N., Biggs, J., Fagereng, Å., Mphepo, F., Dulanya, Z., ... Adams, B. A. (2020). Structural inheritance and border fault reactivation during active early-stage rifting along the Thyolo fault, Malawi. *J. Struct. Geol.*, *139*, 104097. doi: https://doi.org/10.1016/j.jsg.2020.104097

Wessel, B., Huber, M., Wohlfart, C., Marschalk, U., Kosmann, D., & Roth, A. (2018, may). Accuracy assessment of the global TanDEM-X Digital Elevation Model with GPS data. *ISPRS J. Photogramm. Remote Sens.*, *139*, 171–182. doi: 10.1016/j.isprsjprs.2018.02.017

Wheeler, W. H., & Rosendahl, B. R. (1994, apr). Geometry of the Livingstone Mountains Border Fault, Nyasa (Malawi) Rift, East Africa. *Tectonics*, *13*(2), 303–312. doi: 10.1029/93TC02314

Williams, J. N., Fagereng, Å., Wedmore, L. N., Biggs, J., Mphepo, F., Dulanya, Z., ... Blenkinsop, T. (2019). How Do Variably Striking Faults Reactivate During Rifting? Insights From Southern Malawi. *Geochemistry, Geophys. Geosystems*, *20*(7), 3588–3607. doi: 10.1029/2019GC008219

Williams, J. N., Mdala, H., Fagereng, Å., Wedmore, L. N. J., Biggs, J., Dulanya, Z., ... Mphepo, F. (2021). A systems-based approach to parameterise seismic hazard in regions with little historical or instrumental seismicity: active fault and seismogenic source databases for southern Malawi. *Solid Earth*, *12*(1), 187–217. doi: 10.5194/se-12-187-2021

Worthington, R. P., & Walsh, J. J. (2017, jan). Timing, growth and structure of a reactivated basin-bounding fault. In *Geol. soc. spec. publ.* (Vol. 439, pp. 511–531.). Geological Society of London. doi: 10.1144/SP439.14

Yang, Z., & Chen, W. P. (2010, dec). Earthquakes along the East African Rift System: A multiscale, system-wide perspective. *J. Geophys. Res. Solid Earth*, *115*(12). doi: 10.1029/2009JB006779

Zhao, J. X., & Xu, H. (2013). A Comparison of VS30 and Site Period as Site?Effect Parameters in Response Spectral Ground?Motion Prediction Equations. *Bull. Seismol. Soc. Am.*, *103*(1), 1–18. Retrieved from `http://www.bssaonline.org/content/103/1/1.abstract` doi: 10.1785/0120110251

Zielke, O., Schorlemmer, D., Jónsson, S., & Mai, P. M. (2020, jul). Magnitude-dependent transient increase of seismogenic depth. *Seismol. Res. Lett.*, *91*(4), 2182–2191. doi: 10.1785/0220190392